NASA Contractor Report 189076
AIAA–92–0376

Unsteady Blade Pressures on a Propfan at Takeoff: Euler Analysis and Flight Data

M. Nallasamy
Sverdrup Technology, Inc.
Lewis Research Center Group
Brook Park, Ohio

November 1991

Prepared for
Lewis Research Center
Under Contract NAS3–25266

National Aeronautics and
Space Administration

UNSTEADY BLADE PRESSURES ON A PROPFAN AT TAKEOFF: EULER ANALYSIS AND FLIGHT DATA

M. Nallasamy*
Sverdrup Technology, Inc.
Lewis Research Center Group
Brook Park, Ohio 44142

Abstract

The unsteady blade pressures due to the operation of the propfan at an angle to the direction of the mean flow are obtained by solving the unsteady three-dimensional Euler equations. The configuration considered is the eight-bladed SR7L propfan operating at takeoff conditions and the inflow angles considered are 6.3°, 8.3°, and 11.3°. The predicted blade pressure waveforms are compared with in-flight measurements. At the inboard radial station ($r/R = 0.68$) the phase of the predicted waveforms shows reasonable agreement with the measurements while the amplitudes are over-predicted in the leading edge region of the blade. At the outboard radial station ($r/R = 0.95$), the predicted amplitudes of the waveforms on the pressure surface are in good agreement with flight data for all inflow angles. The measured (installed propfan) waveforms show a relative phase lag compared to the computed (propfan alone) waveforms. The phase lag depends on the axial location of the transducer and the surface of the blade. On the suction surface, in addition to the relative phase lag, the measurements show distortion (widening and steepening) of the waveforms. The extent of distortion increases with increase in inflow angle. This distortion seems to be due to viscous separation effects which depend on the azimuthal location of the blade and the axial location of the transducer.

Introduction

The enhanced fuel efficiency characteristics of the propfans over the conventional propellers were demonstrated by NASA through its Advanced Turboprop Project.[1] Further improvement in fuel efficiency, noise reduction and structures may result only from a better understanding of the flow features at the design and off-design operating conditions. This understanding is crucial to the improvement of design methodologies for future propfan design.

Flight measurements on a large-scale 9-ft (2.74m) diameter SR7L propfan have provided a unique database of blade stresses, near-field sound pressure levels and blade surface pressures over a range of operating conditions.[2,3] This database may be used to understand the propfan aerodynamic characteristics, validate prediction methods and improve design methodologies. In the flight tests, the propfan was installed on the left wing of a modified instrumented Gulfstream II testbed aircraft. A nacelle tilt arrangement was used to vary the inflow angle to the propfan. Three nacelle tilt angles were considered, -3° and -1° (tilt down) and +2° (tilt up). The effective inflow angle, α, to the propfan however, depends on the airplane angle of attack, nacelle tilt and upwash angle of the flow into the propfan.

The detailed in-flight unsteady blade pressure measurements were made on a specially designed instrumented blade using 30 transducers.[3] The blade suction surface had 20 pressure transducers distributed over three radial stations ($r/R = 0.68$, 0.86 and 0.95, where r is the radial distance and R is the blade tip radius) while the pressure surface had 10 pressure transducers distributed over two radial stations ($r/R = 0.68$ and 0.95). The axial positions of the transducers from the blade leading edge are listed in Table I in terms of normalized chord length, x/c where x is the axial distance and c is the blade chord. Tests were carried out over a range of takeoff and cruise operating conditions.

The unsteady flow features of a propfan at cruise operating conditions were examined by Nallasamy and Groeneweg.[4] They showed that at inflow angles of the order of 5° strong passage shocks extending from suction to pressure surface form and dissolve during each revolution of the blade. They also studied the unsteady flow effects on the blade loading and pressure waveforms at takeoff conditions for an inflow angle of 8.3° (corresponding to a nacelle tilt of -1°)[5], and compared with in-flight measurements. The predicted blade pressure waveforms showed reasonable agreement with flight data at the inboard radial station ($r/R = 0.68$) whereas at the outboard radial station ($r/R = 0.95$) the agreement was poor.

In the present paper the effect of inflow angle on the blade pressure at takeoff operating conditions, Mach number, $M = 0.31$ and advance ratio, $J = 1.6$, is further studied by obtaining unsteady three-dimensional Euler solution for 6.3° and 11.3° inflow

---

* Senior Supervisor, Aeromechanics Department
Member AIAA

angles corresponding to nacelle tilt angles of -3° and +2° respectively, of the flight test.[3] The results obtained here are analyzed together with those obtained for 8.3°,[5] to understand the effect of inflow angle on the blade loading and blade pressure waveforms. The predicted blade pressure waveforms are compared with flight measurements.

Numerical Solution of Unsteady, Three-Dimensional Euler Equations

The unsteady three dimensional Euler equations governing the inviscid flow through a propfan are solved employing a solution procedure developed by Whitfield et al.[6,7] In this procedure the Euler equations in conservative differential form are transformed from a Cartesian reference frame to a body fitted curvilinear reference frame. Then the transformed equations are discretized employing a finite volume technique. An approximate Riemann solver is used for block interface flux definitions and a Lower-Upper (LU) implicit numerical scheme is used to solve the discretized equations. The flowfield is represented by a multiblock composite grid to limit the core memory requirements.

Flow Configuration and Computational Grid

The configuration considered here is that of the eight-bladed SR7L propfan of the flight test.[3] The direction of rotation of the propfan and the axes of reference are shown in Fig. 1. The rotation of the propfan is clockwise, looking downstream and the azimuth angle, Φ, is measured from the z axis as shown. The grid employed here to represent the flowfield is the same as that shown in Fig. 2 of Ref. 5. An H-grid, with 107 × 41 × 13 (axial by radial by circumferential) points in each blade passage is employed. Each blade passage is divided into three blocks with 107 × 41 × 5 grid points in each block. Thus 24 blocks of grid were used to describe the entire flowfield with 456,248 nodal points. Each blade surface is represented by 49 × 27 (axial by spanwise) grid points with higher resolution near the leading and trailing edges, the hub and the tip. Similar grids used with the present solution technique have produced results which are in reasonably good agreement with data.[8,9]

Results and Discussion

The unsteady three dimensional Euler solutions were obtained for the following two flight test cases of Ref. 3: (i) run = 187, id = 3a and nacelle tilt = -3° and (ii) run = 113, id = 3a and nacelle tilt = +2°. The takeoff operating conditions, Mach number = 0.31 and advance ratio = 1.6 are considered. The aircraft angle of attack for these test cases was 5.4°. In addition to nacelle tilt angle and aircraft angle of attack, the upwash angle at the propfan is needed to determine the effective inflow angle.

In the absence of a simple computational procedure to determine the upwash angle, an experimental correlation obtained by Heidelberg and Woodward[10] from their SR7A model propfan test in the NASA Lewis 9 by 15-ft wind tunnel was used to estimate the inflow angle to the propfan. They first measured the pressure response of the blades as a function of inflow angle for the propfan alone configuration. Then a wing was installed downstream of the propfan (as in the flight test case, tractor configuration) and blade pressure response was measured over a range of wing angles of attack and nacelle tilt. It is assumed that the local inflow angle and the propfan angle of attack are the same in the propfan alone case. Then by matching the measured first harmonic response of the blades with wing installation to that of propfan alone configuration, they found the equivalent inflow angle as a function of wing angle of attack (Fig. 13 in Ref. 8). This correlation was obtained for takeoff conditions, Mach number = 0.2, advance ratio = 0.88, and with a straight wing. The same correlation is used here to obtain the effective inflow angle to the propfan. For an aircraft (wing) angle of attack of 5.4°, a nacelle tilt (droop) angle of -3° gives a value of 6.3° for the effective inflow angle, α, (Fig. 1), while a nacelle tilt of +2° gives a value of 11.3°.

The Euler solutions reported here were obtained with inflow angles of 6.3° and 11.3° giving an inflow variation of 5° for a 5° change in nacelle tilt. These solutions are examined together with that obtained for an inflow angle of 8.3° (nacelle tilt = -1°) in Ref. 5, at the same takeoff operating conditions. The present solutions were obtained from an impulse start for three complete revolutions of the propfan, to obtain a reasonably accurate solution. By the third revolution, the results have stabilized as indicated by the periodic variation of per blade power coefficient during the second and third revolutions of the propfan, Fig. 2. The figure shows the variation of the power coefficient with azimuth angle for three inflow angles, for a blade starting at $\Phi = 0$ and executing three complete revolutions ($\Phi = 0$ to 1080°). The results of the third revolution are analyzed and presented here. The predicted total power coefficient (for eight blades) are nearly the same for all three inflow angles and are about 1% higher than the measured value. The expected sinusoidal variation of the blade loading due to inflow angle is clearly observed in all cases. The amplitude of the stabilized power coefficient during the third revolution varies +44

and -42 percent about the mean for $\alpha = 6.3°$, +61 and -53 percent for $\alpha = 8.3°$, and +89 and -68 percent for $\alpha = 11.3°$. For the low inflow angle ($\alpha = 6.3°$) the variation about the mean in the positive and negative directions is nearly the same, as it was also observed in Refs. 5, 9. For higher inflow angles, the difference between the minimum and maximum levels about the mean results directly from the higher positive inflow angles, as a look at the velocity triangles would show.

The harmonic content of the blade loading is obtained by Fourier transforming the blade power coefficient variation during the third revolution of the blade. The power coefficient $C_p = a_o + a_i \cos\omega t + b_i \sin\omega t$, where a_o, a_i, b_i are the Fourier coefficients and t is the time. The loading spectra are shown in Fig. 3. It is seen that the predicted mean blade power coefficient is nearly the same for all three inflow angles and the first harmonic dominates the blade loading. The first harmonic loading lags the blade motion by 3.62°, 3.68° and 3.75° for the three inflow angles, 6.3°, 8.3° and 11.3°, respectively. The relatively low value of lag and the smaller variation with inflow angle are due to the low reduced frequency and flow unsteadiness at the takeoff operating conditions considered here.

The azimuthal variation of the power coefficient, $dC_p/d(r/R)$, are shown in Fig. 4. Figure 4a shows the computed elemental power coefficient variation for an inflow angle of 11.3° at four azimuthal locations, Φ = 0°, 90°, 180° and 270°. Also shown in the figure is the curve for the steady flow ($\alpha = 0°$). The shape of the curve for any azimuthal position is similar to that of the steady flow. The magnitude of the cyclic variation depends on the spanwise location. The elemental power coefficient variation for an inflow angle of 8.3° is shown in Fig. 4b. The trends of the curves with azimuth angle are similar to that of $\alpha = 11.3°$; higher loading levels occur for $\Phi = 180°$ and 270° and lower loading levels for $\Phi = 0°$ and 90° positions. Figure 4c shows the elemental power coefficient variations for $\alpha = 6.3°$. The magnitude of the cyclic variation is small for this inflow angle. At any inflow angle, the maximum deviation (in absolute value) from the steady value occurs at the radial station where the elemental power coefficient attains a maximum, as would be expected from angle of attack variations along the blade span.

The comparisons of the predicted blade pressure waveforms with flight data are presented next, for two inflow angles, $\alpha = 6.3°$ and 11.3°. Such comparisons for $\alpha = 8.3°$ were reported in Ref. 5 and reference to it is made where appropriate. In these waveform comparisons, 0° corresponds to the (top-dead-center) vertical direction for aircraft installation as in the presentation of flight data in Ref. 3. At the outset, it should be mentioned that for the takeoff operating conditions considered here, the flight data do not indicate the formation of a leading edge vortex. During the flight test no steady measurements were made. However, some steady pressure data were obtained during the unsteady pressure test by retaining the DC component of the pressure signal. These data do not indicate the formation of a leading edge vortex. When a leading edge vortex is present[9], the pressure waveforms on the suction surface show double hump form which is absent in the measured waveforms for the present cases, thus suggesting the absence of the vortex(see the waveforms and discussion below).

Figure 5 shows the unsteady blade surface pressure as a function of azimuth angle for the transducer locations on the suction surface at $r/R = 0.68$ for $\alpha = 6.3°$. The measured and predicted waveforms indicate that the response is the largest near the leading edge and the response reduces gradually towards the trailing edge. The predicted phases of the waveforms are in close agreement with data. However, the amplitudes are overpredicted, the maximum overprediction in absolute value occuring near the leading edge. The pressure waveforms for the four transducer locations on the pressure surface at this radial station are shown in Fig. 6. Here again, the phases of the predicted waveforms agree quite well while the amplitudes are overpredicted.

The pressure waveforms at the outboard radial station $r/R = 0.95$ for $\alpha = 6.3°$ are shown in Fig. 7 and 8. Figure 7 shows the pressure waveforms on the suction surface. Even at this radial station, the prediction shows that the largest response occurs near the leading edge and reduce gradually towards the trailing edge. The measurements, however, indicate that the maximum response occurs at $x/c = 0.42$. For this and the transducer at $x/c = 0.58$, the magnitudes are severely underpredicted. The measured waveform is distorted from the linear sinusoidal form of the predicted one. The waveform distortion may occur due to viscous effects manifested in the form of a small separation bubble as suggested by the low pressure (within the bubble) at $\Phi \sim 180°$ for $x/c = 0.42$ and 0.58 and steep rise in pressure (outside the bubble) at about $\Phi = 270°$. The phases of the waveform also differ from the flight data. For all the transducer locations, the measured waveform shows a relative phase lag compared to the Euler solution. This phase lag also attains a maximum at $x/c = 0.42$. This phase lag seems to be the result of an installation effect, that is, the presence of the wing in the flight tests as compared to the propfan alone configuration of the computation. Heidelberg and Woodward[10] noted similar phase variations in their

model tests in the wind tunnel with and without wing installation. They show a relative phase lag of 11° with the wing installation for $\alpha = 10°$ when compared to the propfan alone case at a transducer location $r/R = 0.75$ and $x/c = 0.1$ on the suction surface of the model, while the magnitudes are nearly the same. The phase lag observed here ranges from 4° near the leading edge ($x/c = 0.05$) to about 60° at $x/c = 0.42$. On the pressure side (Fig. 8), however, the magnitudes are well predicted, but the relative phase lag exists at all the transducer locations and it ranges from 15° to 50°. It should be noted here that the comparison of the waveforms predicted using the same solution technique with the propfan alone wind tunnel measured waveforms in Refs. 8,9 did not show any such phase lags.

The pressure waveforms for an inflow angle of 8.3° presented in Ref. 5 showed similar behavior at the outboard radial station. There the phase lag varied from 8° to 30° on the suction surface and from 20° to 38° on the pressure surface.

Next, the pressure waveforms for $\alpha = 11.3°$ are presented for the two radial stations. At the inboard radial station, both the predicted and measured pressure waveforms on the suction surface show that the maximum response occurs near the leading edge ($x/c = 0.05$) and reduces gradually towards the trailing edge. At $x/c = 0.05$ both magnitude and phase are in good agreement with flight measurements. At other transducer locations, the amplitude is overpredicted, the maximum overprediction occuring at $x/c = 0.15$. On the pressure surface (Fig. 10), the predicted waveforms agree well in phase compared to measurements, while the amplitudes are overpredicted.

At the outboard radial station $r/R = 0.95$, the pressure waveforms on the suction surface are shown in Fig. 11 for $\alpha = 11.3°$. First, it is observed that the measured waveforms are distorted from sinusoidal form by broadening and steepening. This distortion increases with increase in inflow angle, 6.3° to 11.3°. At $\alpha = 11.3°$, the maximum distortion appears at $x/c = 0.25$ transducer location. As noted earlier, the distortion of the waveform may be the result of viscous separation. The measured waveform at $x/c = 0.05$ shows a relative phase lead compared to the computed (propfan alone) waveform, but at all other transducer locations a phase lag ranging from 15° to 55° is observed. On the pressure surface at this radial station the predicted waveforms (Fig. 12) show very good agreement in magnitude with measurements (except at $x/c = 0.92$). But a relative phase lag of the measured waveforms ranging from 7° to 30° is observed. At $x/c = 0.92$ the blade response is low and the predicted waveform is 180° out of phase with that of flight measurement. This appears to be due to the strong interaction of the blade-wake and tip-vortex flows and it is not clear as to the kind of interaction that would produce such a phase variation.

Concluding Remarks

The unsteady blade surface pressures due to the operation of the propfan at an angle to the mean flow direction were obtained by solving the three-dimensional Euler equations. Three positive inflow angles, $\alpha = 6.3°$, 8.3° and 11.3° were considered. The predicted waveforms at the inboard radial station show reasonable agreement with in-flight measurements. At the outboard radial station, the measured waveforms show a relative phase lag compared to the measured ones. This phase lag is due to the installation effects, that is, the installed propfan of the flight test compared to the propfan alone configuration of the computation. On the suction surface the measured waveforms also show distortion (widening and steepening) which increases with inflow angle. This distortion appears to be due to viscous effects which are not considered here. Higher flow resolution near the tip region and consideration of the viscous effects may improve the prediction at the outboard stations.

Acknowledgement

This work is sponsored by NASA Lewis Research Center under contract NAS3-25266 with John F. Groeneweg as Project Manager.

References

1. Hager, R.D., and Vrabel, D., "Advanced Turboprop Project", NASA SP-495, 1988.

2. Little, B.H., Poland, D.T., Bartel, H.W., Withers, C.C., and Brown, P.C., "Propfan Test Assessment (PTA) Final Project Report", NASA-CR-185138, July 1989.

3. Parzych, D., Boyd, L, Mesissner,W., and Wyrostek, A., "In Flight Measurement of Steady and Unsteady Blade Surface Pressure of a Single Rotation Large Scale Advanced Propfan Installed on the PTA Aircraft", NASA-CR ,to be published, 1991.

4. Nallasamy, M., and Groeneweg, J.F., "Unsteady Euler Analysis of the Flowfield of a Propfan at an Angle of Attack", AIAA-90-0339, also NASA-TM-102426, Jan. 1990.

5. Nallasamy, M., and Groeneweg, J.F., "Unsteady Flowfield of a Propfan at Takeoff Conditions", presented at the 6th International Symposium on Unsteady Aerodynamics, Aeroacoustics, and Aeroelasticity of Turbomachines and Propellers, Notre Dame, Indiana, Sept. 15-19, 1991.

6. Whitfield, D.L., Swafford, I.W., Janus, J.M., Mulac, R.A., and Belk, D.M., "Three Dimensional Unsteady Euler Solutions for Propfans and Counter-Rotating Propfans", AIAA-87-1197, June 1987.

7. Janus, J.M., and Whitfield, D.L., "A Simple Time Accurate Turbomachinery Algorithm with Numerical Solutions of Uneven Blade Count Configuration", AIAA-89-0206, Jan. 1989.

8. Heidelberg, L.J., and Nallasamy, M., "Unsteady Blade Pressure Measurements for the SR-7A Propeller at Cruise Conditions", AIAA-90-4022, also NASA-TM-103606, October 1990.

9. Nallasamy, M., and Groeneweg, J.F., "Unsteady Blade Surface Pressures on a Large-Scale Advanced Propeller: Prediction and Data", AIAA-90-2402, also NASA-TM-103218, July 1990.

10. Heidelberg, L.J., and Woodward, R.P., "Advanced Turboprop Wing Installation Effects Measured by Unsteady Blade Pressure and Noise", AIAA-87-2719, also NASA-TM-100200, Oct. 1987.

Table I Unsteady Pressure Blade Transducer Locations in Flight Test[3]

Radius r/R	Surface	Normalized chord x/c
0.68	Suction	.05 .10 .15 .25 .40 .60 .80
	Pressure	.15 .40 .60 .80
0.86	Suction	.07 .15 .25 .37 .50 .75 .90
0.95	Suction	.08 .25 .42 .58 .75 .92
	Pressure	.08 .25 .42 .58 .75 .92

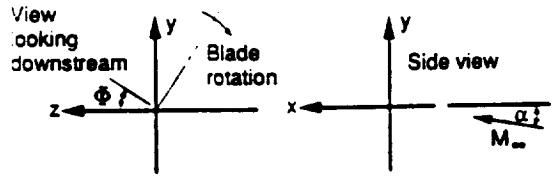

Fig. 1 Reference Coordinates

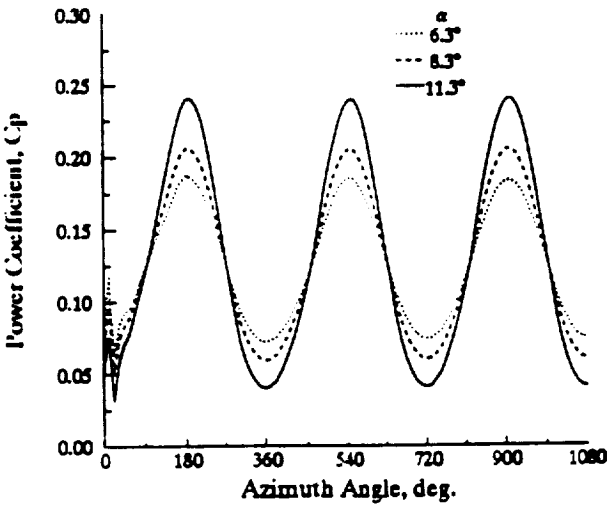

Fig. 2 Power per blade variation with azimuth angle, M = 0.31, J = 1.6

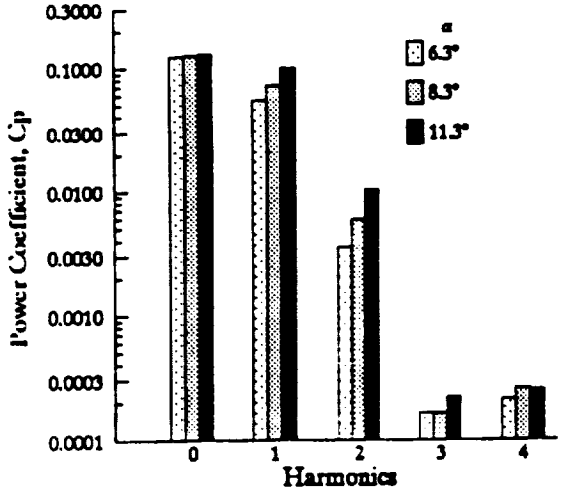

Fig. 3 Loading Spectra, M = 0.31, J = 1.6

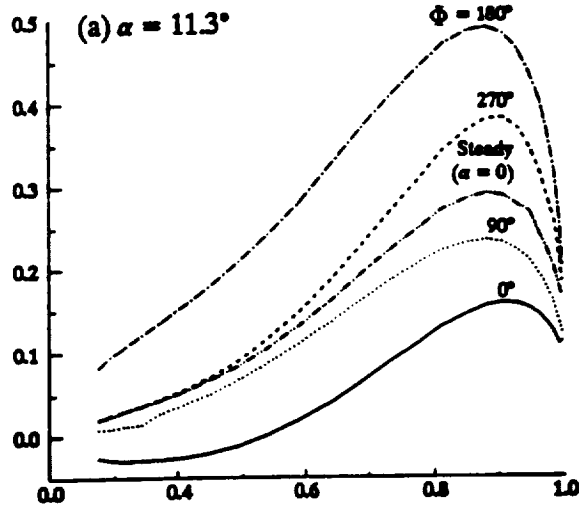

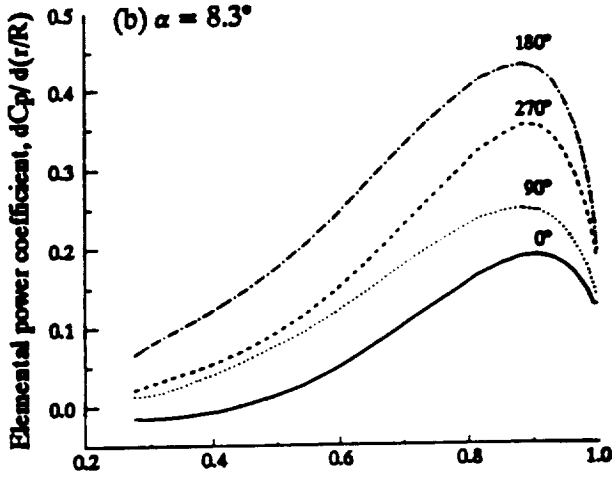

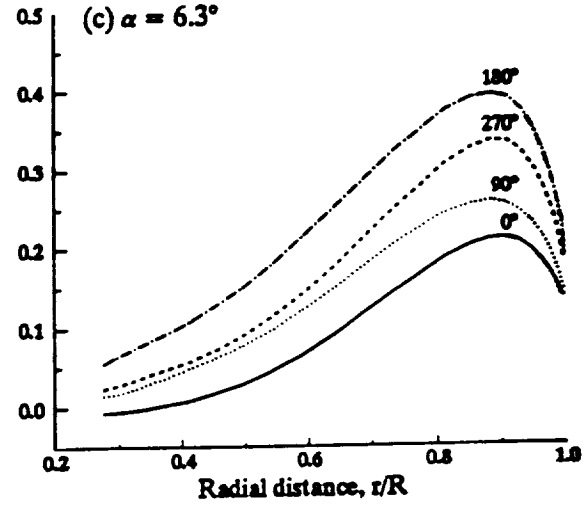

Fig. 4 Elemental power coefficient variation during a revolution, M = 0.31, J = 1.6

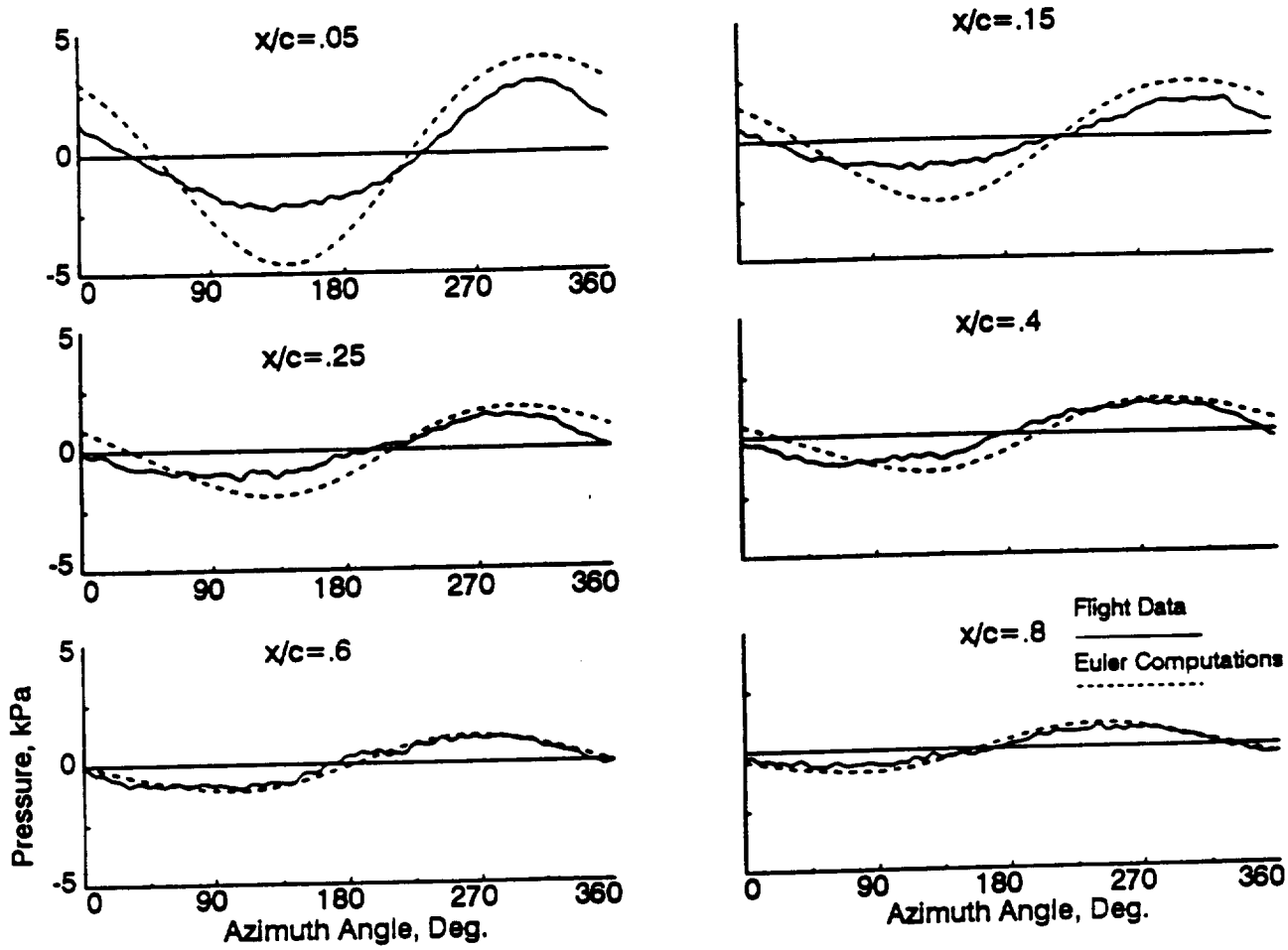

Fig. 5 Pressure Waveforms on the Suction Surface at r/R=0.68, α=6.3°

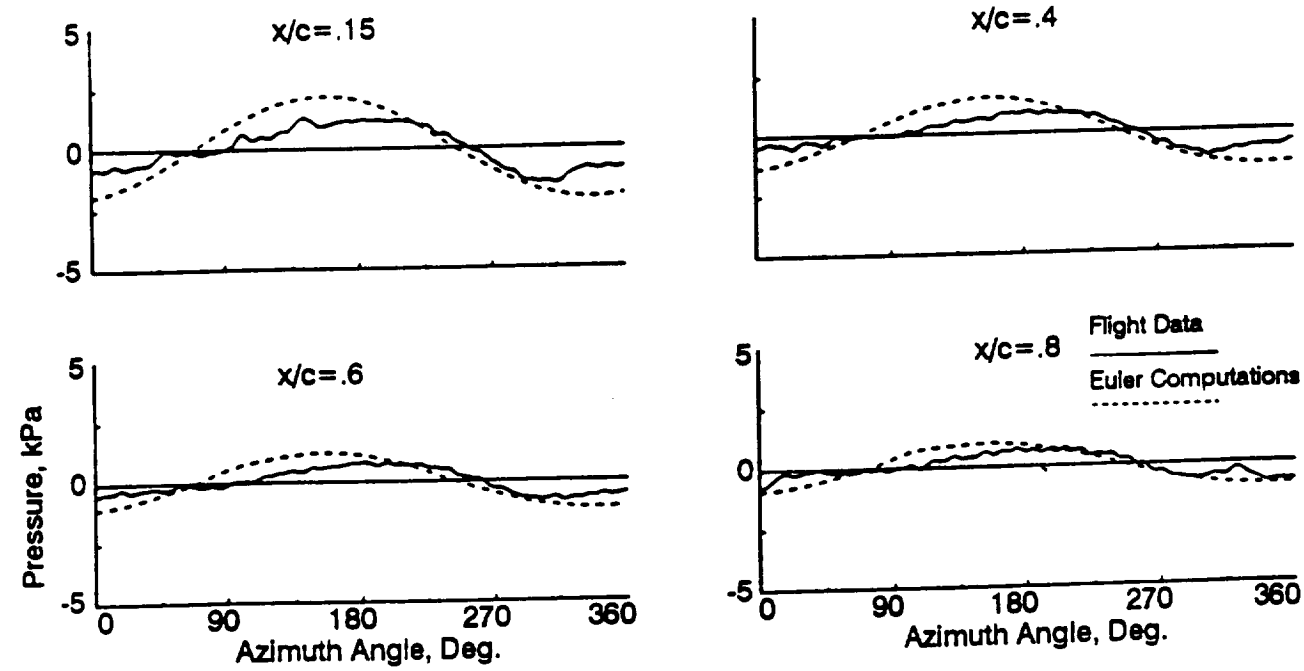

Fig. 6 Pressure Waveforms on the Pressure Surface at r/R=0.68, α=6.3°

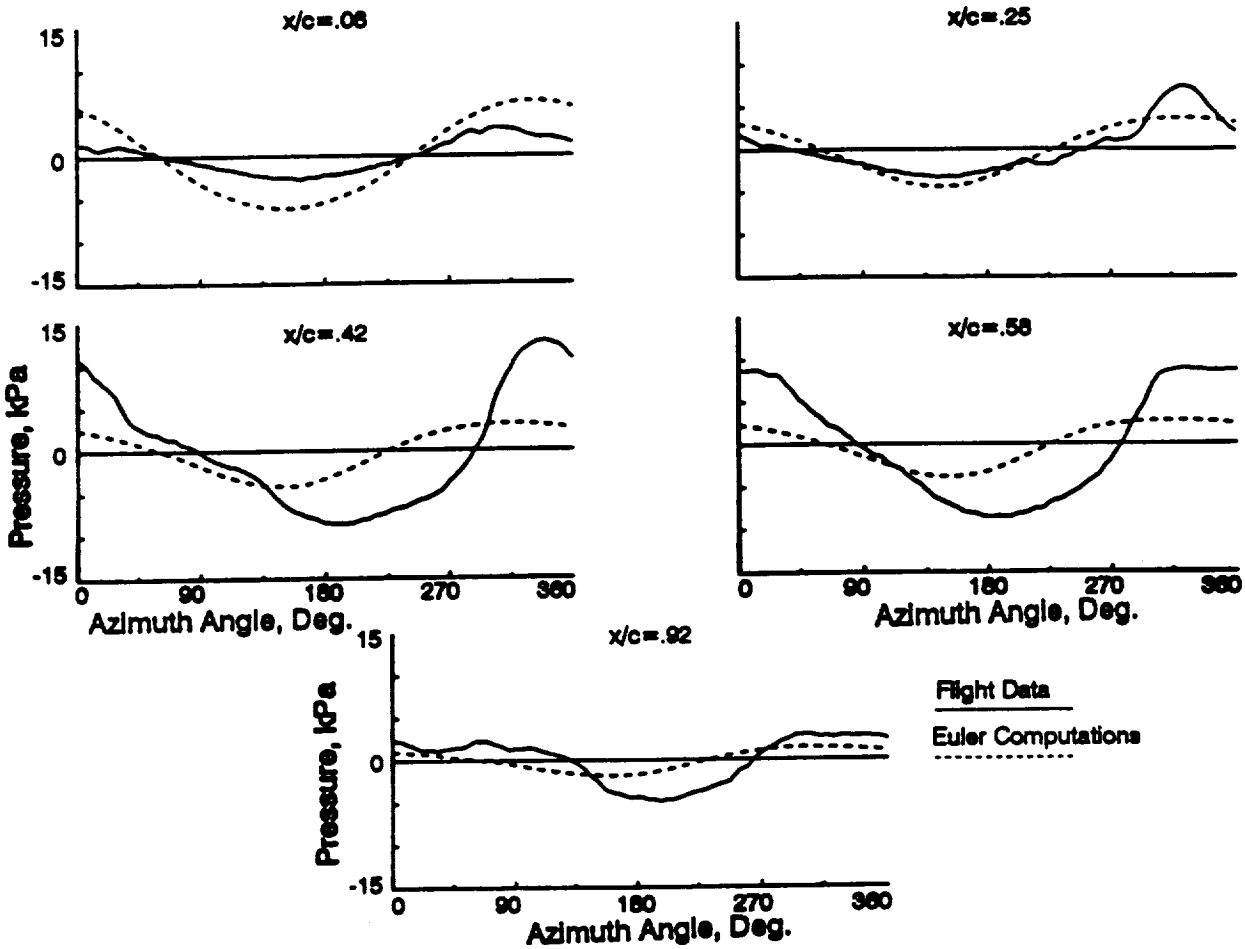

Fig. 7 Pressure Waveforms on the Suction Surface at r/R=0.95, α=6.3°

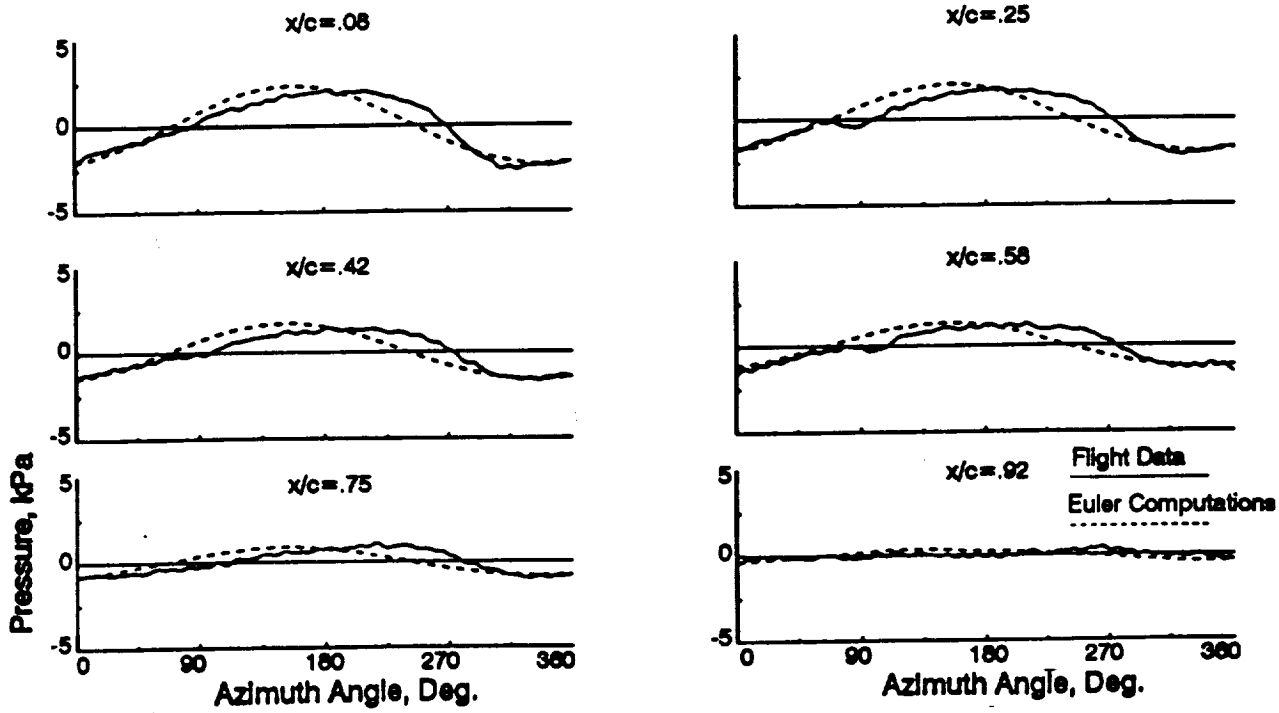

Fig. 8 Pressure Waveforms on the Pressure Surface at r/R=0.95, α=6.3°

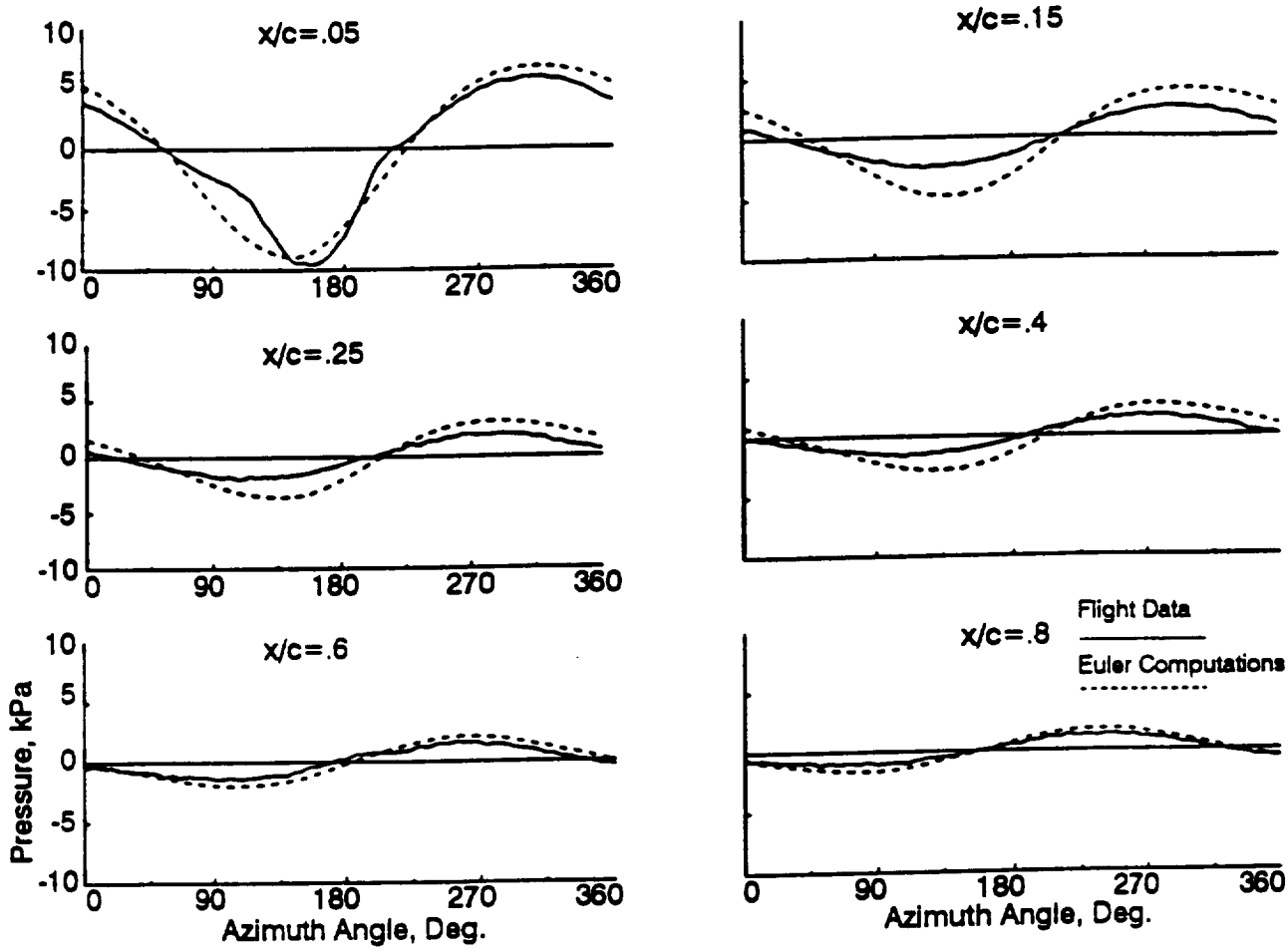

Fig. 9 Pressure Waveforms on the Suction Surface at r/R=0.68, α=11.3°

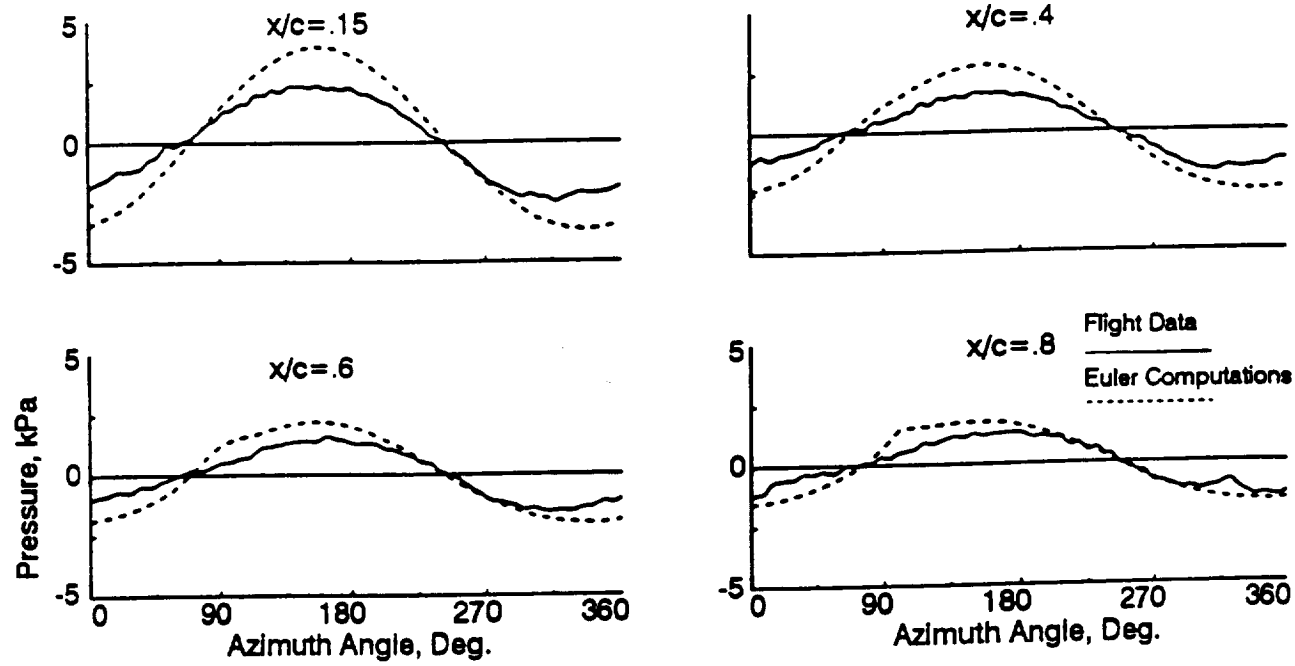

Fig. 10 Pressure Waveforms on the Pressure Surface at r/R=0.68, α=11.3°

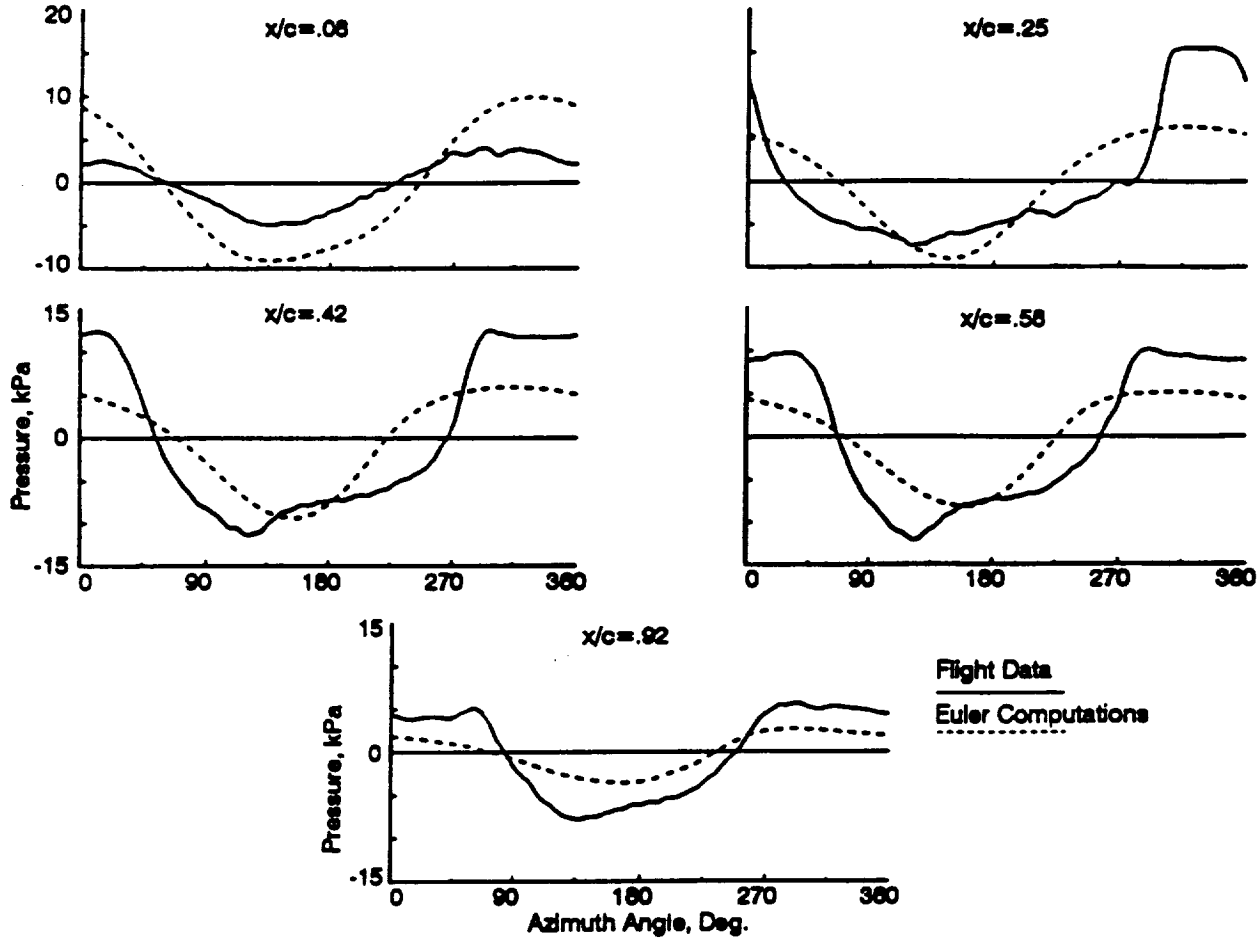

Fig. 11 Pressure Waveforms on the Suction Surface at r/R=0.95, α=11.3°

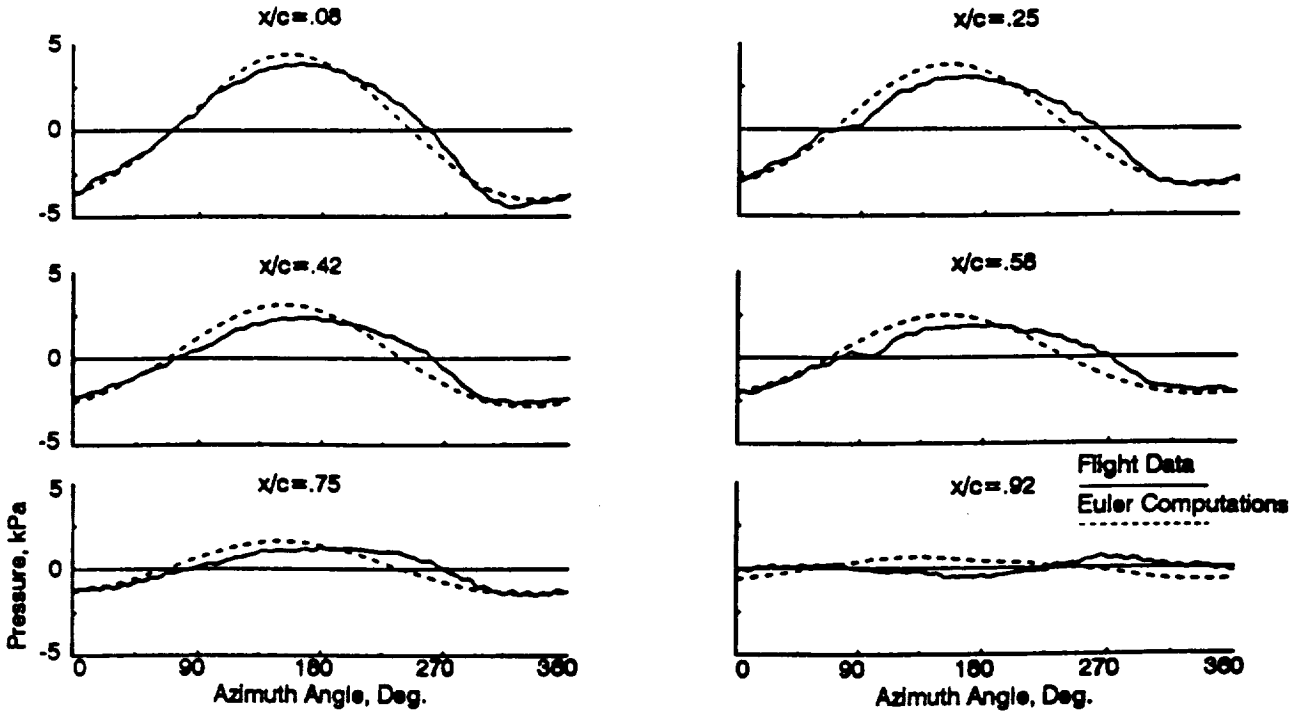

Fig. 12 Pressure Waveforms on the Pressure Surface at r/R=0.95, α=11.3°

REPORT DOCUMENTATION PAGE

Form Approved
OMB No. 0704-0188

1. AGENCY USE ONLY (*Leave blank*)	2. REPORT DATE	3. REPORT TYPE AND DATES COVERED
	November 1991	Final Contractor Report

4. TITLE AND SUBTITLE

Unsteady Blade Pressures on a Propfan at Takeoff:
Euler Analysis and Flight Data

5. FUNDING NUMBERS

WU-535-03-10
C-NAS3-25266

6. AUTHOR(S)

M. Nallasamy

7. PERFORMING ORGANIZATION NAME(S) AND ADDRESS(ES)

Sverdrup Technology, Inc.
Lewis Research Center Group
2001 Aerospace Parkway
Brook Park, Ohio 44142

8. PERFORMING ORGANIZATION REPORT NUMBER

E-6706

9. SPONSORING/MONITORING AGENCY NAMES(S) AND ADDRESS(ES)

National Aeronautics and Space Administration
Lewis Research Center
Cleveland, Ohio 44135-3191

10. SPONSORING/MONITORING AGENCY REPORT NUMBER

NASA CR-189076
AIAA-92-0376

11. SUPPLEMENTARY NOTES

Project Manager, John F. Groeneweg, Propulsion Systems Division, NASA Lewis Research Center, (216) 433-3945. Prepared for the 30th Aerospace Sciences Meeting and Exhibit sponsored by the American Institute of Aeronautics and Astronautics, Reno, Nevada, January 6-9, 1992.

12a. DISTRIBUTION/AVAILABILITY STATEMENT

Unclassified - Unlimited
Subject Categories 71 and 07

12b. DISTRIBUTION CODE

13. ABSTRACT (*Maximum 200 words*)

The unsteady blade pressures due to the operation of the propfan at an angle to the direction of the mean flow are obtained by solving the unsteady three-dimensional Euler equations. The configuration considered is the eight-bladed SR7L propfan operating at takeoff conditions and the inflow angles considered are 6.3°, 8.3°, and 11.3°. The predicted blade pressure waveforms are compared with in-flight measurements. At the inboard radial station (r/R=0.68) the phase of the predicted waveforms shows reasonable agreement with the measurements while the amplitudes are over-predicted in the leading edge region of the blade. At the outboard radial station (r/R=0.95), the predicted amplitudes of the waveforms on the pressure surface are in good agreement with flight data for all inflow angles. The measured (installed propfan) waveforms show a relative phase lag compared to the computed (propfan alone) waveforms. The phase lag depends on the axial location of the transducer and the surface of the blade. On the suction surface, in addition to the relative phase lag, the measurements show distortion (widening and steepening) of the waveforms. The extent of distortion increases with increase in inflow angle. This distortion seems to be due to viscous separation effects which depend on the azimuthal location of the blade and the axial location of the transducer.

14. SUBJECT TERMS	15. NUMBER OF PAGES
Propfan; Unsteady aerodynamics; Computational fluid dynamics	12
	16. PRICE CODE: A03

17. SECURITY CLASSIFICATION OF REPORT	18. SECURITY CLASSIFICATION OF THIS PAGE	19. SECURITY CLASSIFICATION OF ABSTRACT	20. LIMITATION OF ABSTRACT
Unclassified	Unclassified	Unclassified